Spin dynamics and tunneling of the Néel vector in the Fe_{10} magnetic wheel

P. Santini, S. Carretta, and G. Amoretti
Dipartimento di Fisica, Università di Parma, I-43100 Parma, Italy

T. Guidi and R. Caciuffo
Dipartimento di Fisica ed Ingegneria dei Materiali e del Territorio, Università Politecnica delle Marche, Via Brecce Bianche, I-60131 Ancona, Italy

A. Caneschi and D. Rovai
Dipartimento di Chimica, Università di Firenze, UdR INSTM, I-50019 Sesto Fiorentino, Firenze, Italy

Y. Qiu
Department of Materials Science and Engineering, University of Maryland, College Park, Maryland 20742, USA, and NIST Center for Neutron Research, National Institute of Standards and Technology, Gaithersburg, Maryland 20899, USA

J. R. D. Copley
NIST Center for Neutron Research, National Institute of Standards and Technology, Gaithersburg, Maryland 20899, USA
(Received 28 January 2005; published 12 May 2005)

The spin dynamics of a ring-shaped molecule comprising 10 iron(III) ions ($s=5/2$) is studied by inelastic neutron scattering. Exchange integrals and single-ion anisotropy parameters are determined by studying several intermultiplet excitations. Difficulties associated with the dimension of the Hilbert space are overcome by exploiting both the irreducible tensor operator technique and the Lanczos algorithm. By calculating the time correlation function of the Néel vector we show that the low-temperature spin dynamics of Fe_{10} is only approximately described by the semiclassical picture of tunneling of the Néel vector.

DOI: 10.1103/PhysRevB.71.184405 PACS number(s): 75.50.Tt, 75.10.Jm, 75.40.Gb, 75.45.+j

I. INTRODUCTION

Quantum effects in antiferromagnetic (AF) rings formed from a finite number of coplanar magnetic ions were widely investigated during the past few years.[1–11] Indeed, favorable conditions for the observation of mesoscopic quantum coherence are expected in these systems, where tunneling of the Néel vector **n** can take place at a frequency larger than the decoherence rate.[1,3,6]

The Fe_{10} *ferric wheel*, $[Fe(OCH_3)_2(O_2CCH_2Cl)]_{10}$, is a typical example of a spin-compensated AF ring.[12] The ten Fe(III) ions ($s_{Fe}=5/2$) form an almost coplanar ring in a distorted octahedral coordination. With AF nearest-neighbor coupling, the ground state is a singlet with total spin $S=0$. Low temperature magnetization and magnetic torque measurements have revealed the presence of well defined steps at evenly spaced magnetic field values, corresponding to level-crossing conditions.[12–14] Theoretical studies of the low temperature magnetic susceptibility of Fe_{10} are discussed in Ref. 15, and a detailed analysis of the magnetization curves based on numerical simulations, exact diagonalization and density matrix renormalization group methods is given in Ref. 4. A numerical study of the low-lying eigenspectrum of the exchange Hamiltonian for ferric wheels is presented in Ref. 5. Proton nuclear magnetic resonance (NMR) experiments on powder samples have shown a strong enhancement of the spin-lattice relaxation rate T_1^{-1} corresponding to level crossing between $|S,-S\rangle$ and $|S+1,-(S+1)\rangle$ states induced by an external magnetic field.[16] These effects were interpreted as a consequence of dipole-dipole superhyperfine couplings between the proton nuclear spin and the electronic spins of the magnetic ions.[17] Further information on the energy splitting of the low-lying spin levels of Fe_{10} was provided by heat capacity measurements.[18]

Fe_{10} recently attracted interest as a system potentially suitable for observing quantum tunneling of the Néel vector.[1,3] Inelastic neutron scattering (INS) is an ideal technique to assess to what extent such effect characterizes the low-temperature spin dynamics. In fact, the measured change in neutron energy produced by the transition from the Fe_{10} ground state to the first excited spin state gives directly the tunneling frequency of the Néel vector. In addition, from an accurate determination of eigenstates and eigenfunctions of the cluster spin Hamiltonian, the time correlation function of the Néel vector, $\langle n_\alpha(t)n_\alpha(0)\rangle$, can be calculated.

Here we report the results of INS measurements carried out on a polycrystalline sample of Fe_{10}, and we discuss the analysis of the experimental data. Energies and intensities of several excitations corresponding to transitions between zero-field split spin multiplets were observed. Neutron results are interpreted using a microscopic spin Hamiltonian approach, and the dynamics of the Néel vector is analyzed.

II. EXPERIMENTAL DETAILS

The Fe_{10} sample was synthesized following the procedure described in Ref. 12. The molecule has an idealized D_{5d} symmetry, with a C_5 axis passing through the inversion center and five perpendicular C_2 axes passing through pairs of

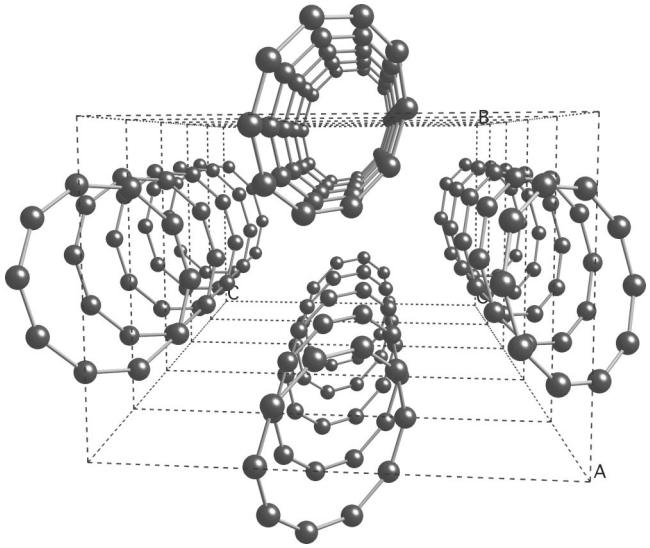

FIG. 1. Perspective view of the Fe_{10} crystal structure. The stacking of the molecules produces channels through the centers of the wheels. Only Fe ions are shown for clarity.

Fe atoms related by the inversion center. The system crystallizes in the $P2_1/c$ space group [$a=11.106(3)$ Å, $b=15.958(3)$ Å, $c=22.938(5)$ Å, $\beta=97.34(1)^\circ$ at 226 K] and the unit cell contains two Fe_{10} molecules related by the 2_1 screw axis (Fig. 1).[12]

The INS experiment was carried out using the time-of-flight Disk Chopper Spectrometer (DCS) at the National Institute of Standards and Technology (NIST) Center for Neutron Research, Gaithersburg, USA.[19] Three grams of protonated polycrystalline sample were sealed in an annular cylindrical Al container, ca. 6 cm in height, 2.2 cm external diameter and 1 mm annular thickness. A standard liquid-helium cryostat allowed us to reach a base temperature of 1.8 K. Data were taken at several temperatures operating DCS in the "low resolution" mode[19] with three incident neutron wavelengths, $\lambda=2.9$ Å, 5 Å, and 7 Å corresponding to full width at half maximum (FWHM) resolution widths for elastic scattering of 500, 105, and 42 μeV, respectively. The measured intensities were normalized to the signal from a vanadium sample and the standard procedure for time-of-flight data treatment was applied using the DAVE software package.[20]

III. EXPERIMENTAL RESULTS AND ANALYSIS

The INS response recorded with an incident neutron wavelength of 7 Å, and the sample at a temperature of 1.8 K, is shown in Fig. 2. Magnetic excitations are observed at 0.33 meV and around 0.67 meV, where two barely resolved peaks can be distinguished. These excitations approximately correspond to transitions from the $|S=0,M=0\rangle$ ground state to the first $|S=1\rangle$ excited state, which is split by anisotropic interactions into its $M=0$, $M=1$ and $M=-1$ components. We attribute the signal at about 0.25 meV to impurities. At 5 K, the intensities of both groups decrease, as expected for transitions arising from the ground state. The splitting of the $|S=1,M=\pm1\rangle$ states suggests the presence of a sizeable non-axial term in the spin Hamiltonian.

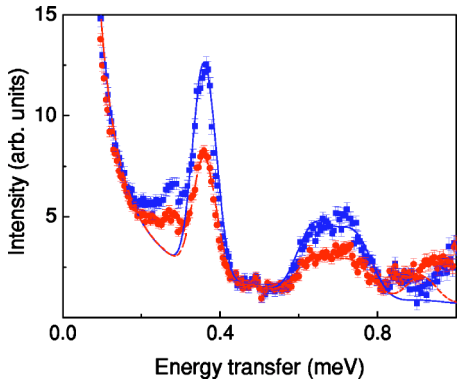

FIG. 2. (Color online) INS spectra recorded on DCS with an incident wavelength of 7 Å and the sample at 1.8 K (blue squares) and 5 K (red circles). Counts in individual detectors at different scattering angles were summed before the time-of-flight to energy conversion. The solid lines represent intensities calculated as described in the text.

Spin excitations at higher energy were measured using an incident wavelength of 5 Å at three different temperatures, 2, 5 and 10 K (Fig. 3). Because of the lower energy resolution in this setup, the spurious peak at 0.25 meV appears as a shoulder on the low-energy side of the peak at 0.33 meV. The peak at 1.20 meV in the spectrum recorded at 2 K is due to a transition from the weakly populated $|S=1,M=0\rangle$ state at 0.33 meV to the $|S=2\rangle$ multiplet, centered at about 1.5 meV. At 5 K the $|S=1,M=\pm1\rangle$ levels are also thermally populated, and the $|S=1,M=\pm1\rangle\rightarrow|S=2\rangle$ transition appears at 0.9 meV. Finally, at 10 K the transition from the $|S=2\rangle$ level to the $|S=3\rangle$ state lying at about 3.1 meV becomes visible at 1.6 meV. Thus the low-lying spin multiplets with $S=1$, 2, 3 … have, to a good approximation, energies given by the Landé interval rule (see below), $E(S)=2JS(S+1)/N$, with $N=10$ and $J=1.25$ meV. The J value so determined has been

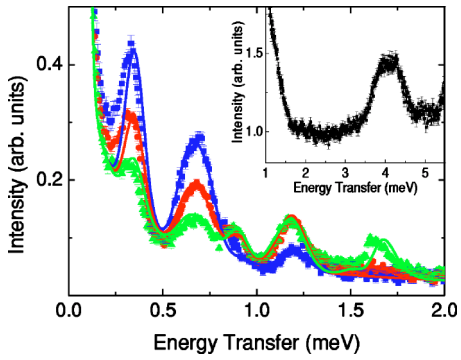

FIG. 3. (Color online) Spectra recorded with $\lambda=5$ Å and $T=2$ K (blue squares), 5 K (red circles), and 10 K (green triangles). The energy resolution is 105 μeV at the elastic peak. Data points correspond to the sum of individual detector counts over the spanned scattering angle range. The solid lines are intensities calculated as described in the text. The inset shows the intensity distribution measured at 1.8 K with an incident neutron wavelength of 2.9 Å.

used as starting point in the fitting procedure of the whole data set.

The spectrum recorded at $T=1.8$ K with $\lambda=2.9$ Å is shown in the inset of Fig. 3. Because of the INS selection rules, $\Delta S=0,\pm1$, the neutron group around 4 meV must correspond to a transition from the $|S=0\rangle$ ground state to $|S=0\rangle$ or $|S=1\rangle$ excited states not belonging to the Landé band. Indeed, the diagonalization of the exchange Hamiltonian allows us to identify this broad peak with transitions toward four, almost degenerate, $|S=1\rangle$ multiplets.

The experimental data were interpreted assuming that the cluster spin system can be described by the Hamiltonian

$$H=J\sum_{i=1}^{10}\mathbf{s}_i\cdot\mathbf{s}_{i+1}+d\sum_{i=1}^{10}\left[s_{z,i}^2-\frac{1}{3}s_i(s_i+1)\right]+e\sum_{i=1}^{10}[s_{x,i}^2-s_{y,i}^2]+\sum_{i<j=1}^{10}\mathbf{s}_i\cdot\mathbf{D}_{ij}\cdot\mathbf{s}_j+g\mu_B\mathbf{B}\cdot\sum_{i=1}^{10}\mathbf{s}_i. \quad (1)$$

The first term, with $\mathbf{s}_{11}\equiv\mathbf{s}_1$, is the isotropic, nearest-neighbor Heisenberg exchange interaction. The second and third terms describe the axial and rhombic parts of the local crystal-field (CF) interaction, and the fourth term is the dipole-dipole intracluster interaction, which is evaluated within the point-dipole approximation. The $\hat{\mathbf{z}}$ axis is normal to the plane of the ring. Fourth-order local anisotropy terms have no appreciable effect on the calculated INS intensities and are therefore neglected.

Since $s_i=5/2$, the total dimension of the Hilbert space is very large, $(2s_i+1)^{10}=60466176$, and this prevents a full exact diagonalization of the Hamiltonian. The Heisenberg contribution is dominant and antiferromagnetic. Hence, as a first approximation, the energy spectrum is characterized by a series of level multiplets with an almost definite value of the total spin quantum number S. Therefore, in the first step of our procedure only the first term in Eq. (1) was considered. By exploiting the rotational invariance of the isotropic exchange interaction, the Hamiltonian matrix was block-factorized according to S. This can be effectively done by using irreducible tensor operators (ITO) algebra, and writing the spin states $|n\rangle$ as linear combinations of basis vectors $|(\tilde{S})SM\rangle$ labelled by the set of intermediate spin states $(\tilde{S})$. A further factorization was achieved by building basis states belonging to irreducible representations (irreps) of the C_2 point group, as the exploitation of the full symmetry of the Heisenberg Hamiltonian turned out to be more cumbersome to treat numerically. Even in this way the dimensions of the diagonal blocks remain too large (of the order of 200000) to perform a full standard diagonalization. Therefore, we used the Lanczos method to calculate the lowest eight states in each subspace, i.e., for each value of S and for each irrep of C_2. By using the Lanczos method in combination with the ITO formalism (which was needed to exploit the conservation of the total spin) we managed to include a number of excited states sufficient to interpret INS results at nonzero temperature. In the second step of our calculation, the anisotropic part of the spin Hamiltonian and the associated S-mixing effects were included by using the procedure described in Refs. 8 and 21. The error associated with this procedure is much smaller than experimental uncertainty.

The lowest energy levels of the Heisenberg part of the Hamiltonian are shown in Fig. 4. The energy of the lowest level for each value of S almost exactly follows the rotational ("L") band behavior,[22,23] $E(S)=A_LS(S+1)$, with $A_L\sim0.25$ meV. These levels belong to the $k=0$ or $k=\pi$ irreps of the discrete translation group. A second group of parabolic bands ("E bands"[9]) is visible above the rotational band. These levels belong to the $k\neq0,\ \pi$ irreps of the discrete translation group. The L and E bands reflect the fact that at low energy the exchange Hamiltonian can be approximated by a two-sublattice Hamiltonian $\propto\mathbf{S}_{\text{even}}\cdot\mathbf{S}_{\text{odd}}$, where $\mathbf{S}_{\text{even}}(\mathbf{S}_{\text{odd}})$ is the total spin of even (odd) sites.[24] The rotational character of the L-band excitations can also be understood by considering that if the spins in the ring have nearly staggered (Néel) alignment the AF Heisenberg Hamiltonian with uniaxial anisotropy can be semiclassically mapped into[1]

$$H_{\text{rot}}=\frac{2J}{N}\mathbf{S}^2+g\mu_B\mathbf{B}\cdot\mathbf{S}+Nd n_z^2, \quad (2)$$

where N is the number of spin centers in the ring, $\mathbf{S}=\mathbf{S}_{\text{even}}+\mathbf{S}_{\text{odd}}$ is the total spin and $\mathbf{n}=(\mathbf{S}_{\text{even}}-\mathbf{S}_{\text{odd}})/N$ is the Néel vector. If $\mathbf{B}=0$ and $d=0$, H_{rot} describes an $O(3)$ rigid rotor, whose eigenvalues are $2JS(S+1)/N$.

The INS cross section for a polycrystalline sample of magnetic molecules is[25]

$$\frac{\partial^2\sigma}{\partial\Omega\,\partial\omega}=\frac{A}{N_m}\frac{k_f}{k_0}e^{-2W}\sum_{n,n'}\frac{e^{-\beta E_n}}{Z}I_{nn'}(Q)\,\delta(\hbar\omega-E_{n'}+E_n), \quad (3)$$

where $A=0.29$ barn and the function $I_{nn'}(Q)$ is defined as[26]

$$I_{nn'}(Q)=\sum_{i,j}F_i^*(Q)F_j(Q)\left\{\frac{2}{3}[j_0(QR_{ij})+C_0^2j_2(QR_{ij})]\tilde{s}_{z_i}\tilde{s}_{z_j}+\frac{2}{3}\left[j_0(QR_{ij})-\frac{1}{2}C_0^2j_2(QR_{ij})\right](\tilde{s}_{x_i}\tilde{s}_{x_j}+\tilde{s}_{y_i}\tilde{s}_{y_j})+\frac{1}{2}j_2(QR_{ij})[C_2^2(\tilde{s}_{x_i}\tilde{s}_{x_j}-\tilde{s}_{y_i}\tilde{s}_{y_j})+C_{-2}^2(\tilde{s}_{x_i}\tilde{s}_{y_j}+\tilde{s}_{y_i}\tilde{s}_{x_j})]+j_2(QR_{ij})[C_1^2(\tilde{s}_{z_i}\tilde{s}_{x_j}+\tilde{s}_{x_i}\tilde{s}_{z_j})+C_{-1}^2(\tilde{s}_{z_i}\tilde{s}_{y_j}+\tilde{s}_{y_i}\tilde{s}_{z_j})]\right\}. \quad (4)$$

In the above equations N_m is the number of magnetic ions, Z is the partition function, $\mathbf{k}_f$ and $\mathbf{k}_0$ are the wave vectors of the scattered and incident neutrons, $\exp(-2W)$ is the Debye-Waller factor, $\mathbf{Q}=\mathbf{k}_0-\mathbf{k}_f$ is the scattering vector, E_n is the energy of the spin state $|n\rangle$, $F(Q)$ is the magnetic form factor, $\mathbf{R}_{ij}$ gives the relative position of ions i and j,

$$C_0^2=\frac{1}{2}\left[3\left(\frac{R_{ijz}}{R_{ij}}\right)^2-1\right],$$

$$C_2^2=\frac{R_{ijx}^2-R_{ijy}^2}{R_{ij}^2},$$

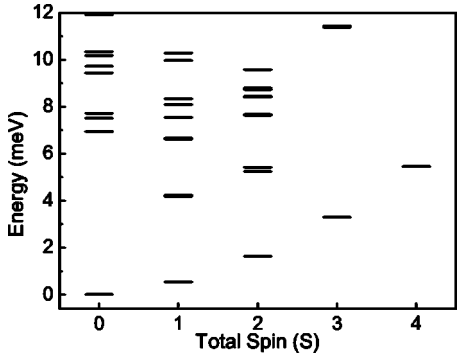

FIG. 4. Lowest energy multiplets of the Heisenberg part of the Hamiltonian as a function of the total spin S.

$$C_{-2}^2 = 2\frac{R_{ijx}R_{ijy}}{R_{ij}^2},$$

$$C_1^2 = \frac{R_{ijx}R_{ijz}}{R_{ij}^2},$$

$$C_{-1}^2 = \frac{R_{ijy}R_{ijz}}{R_{ij}^2}, \tag{5}$$

and

$$\tilde{s}_{\alpha_i}\tilde{s}_{\gamma_j} = \langle n|s_{\alpha_i}|n'\rangle\langle n'|s_{\gamma_j}|n\rangle \ (\alpha,\gamma = x,y,z). \tag{6}$$

A best fit of the measured neutron spectra based on calculations of Eq. (3) enables the parameters of the spin Hamiltonian to be determined. The analysis is here complicated by the fact that even at low temperature the INS spectra show a broadening of the inelastic features, whose FWHM is about twice as large as the instrument resolution. This broadening is most probably a consequence of structural disorder resulting in a spread of the anisotropy parameters throughout the sample. To account for this effect in the simplest possible way, the CF parameters d and e [cf. Eq. (1)] were allowed to vary within a finite interval assuming Gaussian distributions of values. These distributions were then used to obtain a weighted average of the INS spectra calculated for different sets of parameters, assuming resolution limited linewidths for each set. The best fit of the experimental data (solid lines in Figs. 2 and 3) is obtained for a nearest-neighbor exchange integral $J=1.23$ meV, an axial anisotropy parameter with mean value $d=-5$ μeV and standard deviation $\sigma_d=0.25$ μeV, and a rhombic anisotropy parameter with mean value $e=3.6$ μeV and standard deviation $\sigma_e=1.8$ μeV. An almost equivalent fit is obtained assuming the values of d quoted above and values of e approximately halved. There are in fact two sources of axial and in-plane anisotropies, namely crystal field and dipole-dipole interactions. While the sign of the axial anisotropy can be deduced from the measured spectra, no information can be extracted about the sign of the in-plane anisotropy. Hence, once the dipole-dipole contribution is calculated in the point-dipole approximation, there are two possible choices for e fitting the spectra equally well. We remark that the CF axial anisotropy, represented by the parameter d, is about 30% of the total, the dominant contribution being determined by the dipole-dipole interactions. For a realistic modelling of disorder one should include the distribution of dipole-dipole interaction strengths produced by local strains. We have instead chosen to mimic the latter by a wider distribution of CF parameters for the sake of simplicity, since this choice turns out to work very well and it does not affect the mean values of the best-fit parameters.

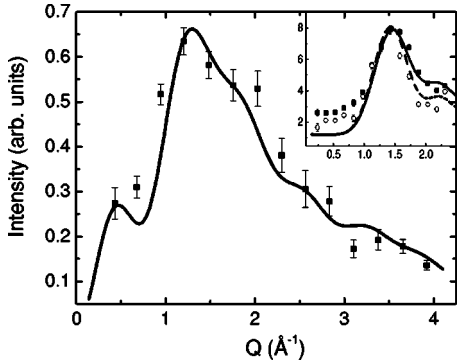

FIG. 5. Neutron scattering intensities for the transition $|S=0\rangle \rightarrow |S=1\rangle$ at 4 meV, as a function of the transferred wave vector Q ($\lambda=2.9$ Å). The line is the corresponding calculated intensity. The inset shows the Q dependence of the $|S=0,M=0\rangle \rightarrow |S=1,M=0\rangle$ transition at 0.33 meV (open circles and dashed line) and $|S=0,M=0\rangle \rightarrow |S=1,M=\pm 1\rangle$ transition at 0.67 meV (squares and solid line); ($\lambda=5$ Å).

Equation (3) has also been used to evaluate the Q dependence of the transition intensities obtained from groups of detectors after normalization for efficiency and geometrical variations. The experimental data for selected transitions are shown in Fig. 5 together with the calculated curves. The good agreement between calculation and experiment confirms the proposed spectroscopic assignment.

IV. DYNAMICS OF THE NÉEL VECTOR

The low-T, low-frequency spin dynamics of Fe_{10} can be expressed in terms of the dynamics of the Néel vector $\mathbf{n}(t)$ and the total spin $\mathbf{S}(t)$.[6] In fact, since low-energy states belong to either the $k=0$ or the $k=\pi$ irreps of the discrete translation group of the ring, at low T the low-frequency spectrum of the various dynamical spin correlations is solely determined by the dynamical structure factors of **S** and **n**.

The most interesting aspect of the dynamics of Fe_{10} is the possible occurrence of tunneling of the direction of **n**.[1,3,6] This is the AF counterpart of the tunneling of the magnetization (S_z in the present notation) observed in nanomagnets (e.g., Mn_{12} or Fe_8). For the latter the tunneling time is macroscopic, and so long that the time autocorrelation of S_z becomes overdamped due to dissipation into the nuclear-spins subsystem. Thus the temporal oscillations of S_z associated with coherent tunneling do not actually take place. On the contrary, the time scale of the tunneling of **n** in AF rings is microscopic, and much shorter than the decoherence time associated with spin-nuclei or spin-phonon interactions.

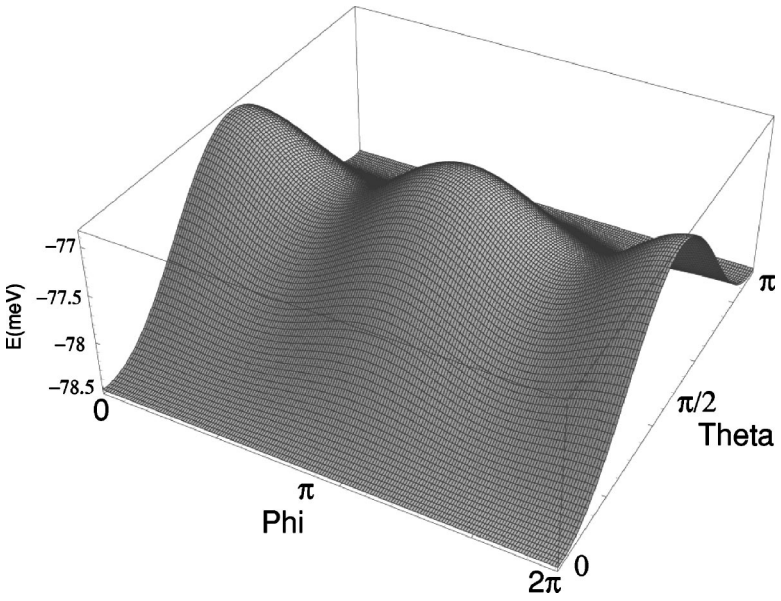

FIG. 6. Classical energy $E(\theta,\phi)$ as a function of the direction (θ,ϕ) of the spin of one sublattice in the presence of an external magnetic field $B=6.6$ T applied along the $\hat{\mathbf{x}}$ direction (see text).

Within the semiclassical framework of Eq. (2), the condition for the occurrence of a tunneling regime is that the tunnel action $\mathcal{S}_0=Ns\sqrt{-2d/J}$ be much larger than unity.[6] With this condition, the orientation of the vector **n** tunnels between $\pm\hat{\mathbf{z}}$. The estimate for the tunnel action in Fe_{10} (based on torque measurements results) was $\mathcal{S}_0=3.3$,[4,6] making this ring one of the most promising candidates for the tunneling to be observed. Our neutron scattering results show that $\mathcal{S}_0$ is even larger, i.e. $\mathcal{S}_0\sim 4.2$. In order to match the semiclassical description, in calculating $\mathcal{S}_0$ we considered a model Hamiltonian given by Eq. (1), simplified by assuming single-site axial anisotropy only, but with a larger value of the axial parameter, $d^*=3.45d=-17$ μeV.[27] The previous underestimate of $\mathcal{S}_0$ was due to both an overestimation of J and an underestimation of d^*. Indeed, the parameters used in Ref. 4 are $J=1.34$ meV and $d^*=-12$ μeV.

In order to illustrate the classical situation, we consider the classical version of the model Hamiltonian given by Eq. (1).[27] The magnetic field **B** is applied along the $\hat{\mathbf{x}}$ direction. Figure 6 shows the energy surface $E(\theta,\phi)$ as a function of the direction (θ,ϕ) of the spin of one sublattice. For any value of (θ,ϕ) the orientation of the second sublattice is determined by minimizing the classical energy. Classically, there are two equivalent minima in $E(\theta,\phi)$, which correspond to swapping the two sublattices. These minima are separated by an energy barrier at $\theta=\pi/2$, whose height and shape can be modulated by varying the field intensity B. For $B=0$ the minima are at $\theta=0$ and $\theta=\pi$, the barrier is at $\theta=\pi/2$ and its height is independent of the value of ϕ. For $B\neq 0$ canting along $\hat{\mathbf{x}}$ occurs, the minima are displaced from $\theta=0$, π and there are saddle points at $\theta=\pi/2$ and $\phi\neq 0$. The height of the energy barrier is

$$U = Nd^*\left(\frac{(g\mu_B B)^2}{16J^2 - 8Jd^*} - s^2\right). \tag{7}$$

This gives $U=1.078$ meV for $B=0$ and $U=1.074$ meV for $B=6.6$ T. Hence, at $T=0$, **n** is fixed at one of the two minima.

The quantum behavior of the model is very different from the classical one. Figure 7 shows the energy levels of the Hamiltonian Eq. (1) as a function of B. The ground state $|0\rangle$ is nondegenerate, except at level-crossing fields. Since the observable **n** does not commute with H, it experiences quantum fluctuations that are described by the $T=0$ autocorrelation functions,[6]

$$\langle n_\alpha(t)n_\alpha(0)\rangle = \sum_\nu e^{-i\Delta_\nu t/\hbar}|\langle\nu|n_\alpha|0\rangle|^2, \tag{8}$$

where $|\nu\rangle$ is the νth spin level, $\Delta_\nu=E(\nu)-E(0)$ and $\alpha=x,y,z$. Hence, in principle many different frequencies may contribute to the Néel-vector dynamics.

The spectral weight $|\langle 1|n_z|0\rangle|^2$, corresponding to the lowest frequency Δ_1, is calculated as a function of B and compared in Fig. 8(a) with the sum of all remaining higher-frequency weights, $W_{\nu>1}=\Sigma_{\nu\neq 1}|\langle\nu|n_z|0\rangle|^2$. The dynamics of the Néel vector is characterized by single-frequency oscillations only for B values corresponding to vanishingly small $W_{\nu>1}$. This situation occurs for $B=0$ and for B values which are intermediate between two consecutive ground-state crossing fields (i.e., corresponding to *anti*crossings between the first and second excited states), as can be immediately

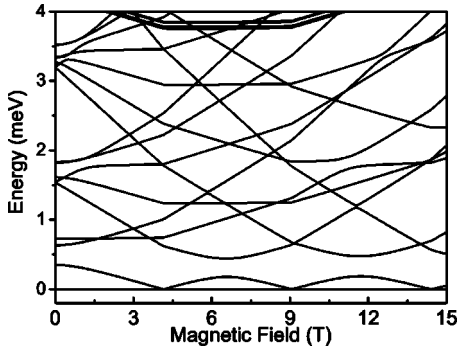

FIG. 7. Energy levels of the Hamiltonian Eq. (1) as a function of an external magnetic field B applied along the $\hat{\mathbf{x}}$ direction.

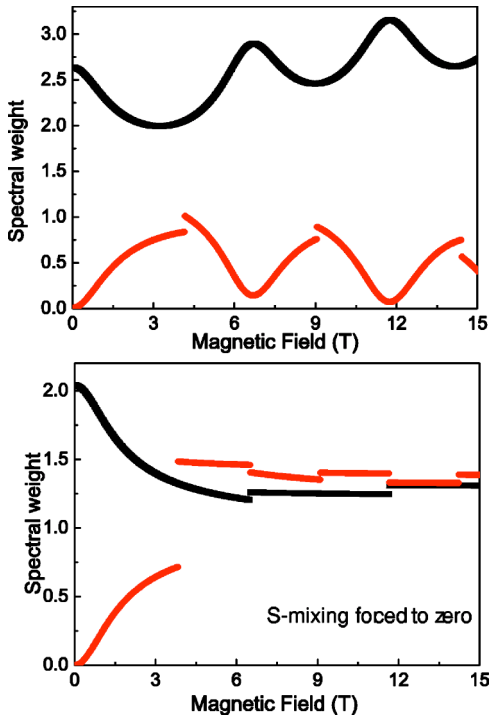

FIG. 8. (Color online) (Upper panel) Magnetic-field dependence of $|\langle 1|n_z|0\rangle|^2$ (black) compared with $\Sigma_{\nu\neq 1}|\langle \nu|n_z|0\rangle|^2$ (red), calculated from the full Hamiltonian Eq. (1). The magnetic field is oriented along $\hat{\mathbf{x}}$. (lower panel) The same quantities calculated with S mixing forced to zero.

verified by inspection of Fig. 7. Similar results were obtained for Fe_6 and Fe_8 in Ref. 6. Hence, at these particular values of B (including $B=0$), the autocorrelation of n_z oscillates with a single frequency. Since this single frequency ($\lesssim 0.35$ meV) is smaller than the classical energy barrier (~ 1.07 meV), this situation recalls the semiclassical image of tunneling of n_z.

For $B=0$, the existence of a single dominating frequency in the dynamics of n_z can be understood on the basis of general considerations on AF bipartite rings. In fact, in small rings of this type, the exchange part of the Hamiltonian can be approximated by a 2-sublattice Hamiltonian $\propto \mathbf{S}_{\text{even}}\cdot\mathbf{S}_{\text{odd}}$. A local spin operator $\mathbf{s}_i$, being of rank 1, connects the ground state only with states having total spin $S=1$. In addition, within the 2-sublattice approximation, these $S=1$ states must belong to either the Landé band or the E band.[24] This holds for $\mathbf{n}$ too, since this observable is a linear combination of local spin operators. In addition, $\mathbf{n}$ has a well-defined wave vector $k=\pi$, and therefore it only connects states whose wave vectors differ by π. As a result, matrix elements $\langle 0|\mathbf{n}|\nu\rangle$ are appreciable only if $|\nu\rangle$ belongs to the $|S=1\rangle$ multiplet of the Landé band. At $B=0$ biaxial anisotropy splits this $|S=1\rangle$ multiplet into a singlet and a quasidoublet. The matrix element $\langle 0|n_z|\nu\rangle$ is nonzero when $|\nu\rangle$ is the singlet $|S=1,M=0\rangle$, whilst $\langle 0|n_{x,y}|\nu\rangle$ are nonzero when $|\nu\rangle$ is one specific state of the doublet $(|S=1,M=1\rangle \pm |S=1,M=-1\rangle)/\sqrt{2}$. Hence, in a bipartite AF ring, the autocorrelation function of all three components of $\mathbf{n}$ is expected to be characterized by a single dominating frequency at $B=0$ but, as we will see below, this condition is not sufficient for a tunnelling picture to apply.

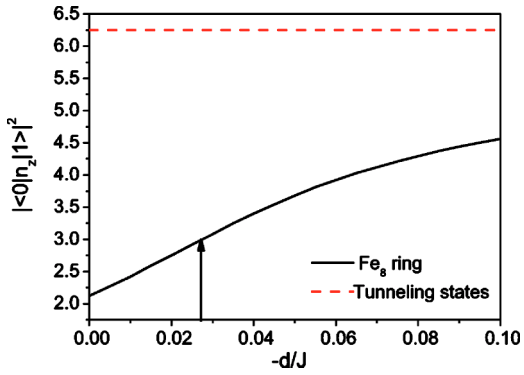

FIG. 9. (Color online) $|\langle 1|n_z|0\rangle|^2$ (black) compared with the corresponding tunneling limit (dashed red) as a function of d/J for an eight sites $s=5/2$ ring (with $B=0$). In-plane and dipolar anisotropies are neglected. The arrow indicates the d/J ratio corresponding to $CsFe_8$ (Ref. 10).

INS data permit a complete determination of the autocorrelation of $n_z \sim |\langle 0|n_z|1\rangle|^2 \exp(-i\Delta_1 t/\hbar)$. In fact, both the tunneling frequency (i.e., the INS peak position) and the matrix element $\langle 0|n_z|1\rangle$ can be extracted from the data. The latter can be obtained by the intensity of the lowest INS peak measured in absolute units, or else by the ratio of the intensities of the two lowest INS peaks. We followed the second way, taking into account the sample inhomogeneity by a proper model (see above). We obtain $\langle 0|n_z|1\rangle = 1.6$ for the ideal homogeneous Fe_{10} molecule. Because of the high spatial symmetry of ideal ring molecules, the momentum transfer (Q) dependence of the powder INS intensity can be calculated analytically,[25] and it is completely specified by the difference Δk in the ring wave vector k of the two states involved in the INS transition. Hence, the structure factor of the INS peak corresponding to the transition between the tunnel-split doublet should follow the behavior expected for $\Delta k=\pi$. This is confirmed by our data and calculations reported in Fig. 5.

Although in Fe_{10} the semiclassical criterion for the validity of the tunneling picture is approximately fulfilled (in fact the tunnel action is $\mathcal{S}_0=4.2$), the actual validity of this picture can be directly assessed by using the measured intensity of the lowest INS peaks to extract the spectral weight $|\langle 0|n_z|1\rangle|^2$. In the ideal tunneling scenario, in which the two states involved in the transition are even and odd combinations of the classical Néel states (i.e., $1/\sqrt{2}(|\uparrow,\downarrow,\uparrow,\ldots\rangle \pm |\downarrow,\uparrow,\downarrow,\ldots\rangle)$, the squared matrix element $|\langle 0|n_z|1\rangle|^2$ should be equal to $s^2=6.25$. This value would be obtained in the limit $-N^2 d \gg J$. In Fe_{10}, the maximum of $|\langle 0|n_z|1\rangle|^2$ varies between about 2.6 and 3.2 (see Fig. 8), so that an ideal tunneling scenario is not achieved. This is also the case for the $CsFe_8$ ring, which has been reported to be one of the best candidate molecules for the tunneling regime to occur.[3] Indeed, although the tunnel action of $CsFe_8$ is

large, $\mathcal{S}_0=4.6$,[10] the value of $|\langle 0|n_z|1\rangle|^2$ for this system is much closer to the isotropic limit ($d=0$) than to the tunneling limit. This can be readily appreciated from Fig. 9, where $|\langle 0|n_z|1\rangle|^2$ is shown as a function of the ratio d/J for an octanuclear $s=5/2$ regular ring. In spite of the fact that the semiclassical picture for the tunneling states is not quantitatively correct, for appropriate values of the applied field (including $B=0$) the autocorrelation of **n** remains nearly monochromatic.

Classical tunneling states are recovered for large values of d, and imply a large degree of S mixing. Even for values of d close to the one we find for Fe_{10}, S mixing plays an important role. First of all, at $B=0$ it increases the weight $|\langle 0|n_z|1\rangle|^2$ by about 30%. This is reflected directly in the relative intensity of the three lowest $|S=0\rangle \rightarrow |S=1\rangle$ transitions: while the transition probability of the lower-lying $|S=0\rangle \rightarrow |S=1, M=0\rangle$ transition is increased by about 30%, the two others are decreased by about 14%. More remarkably, for $B\neq 0$ S mixing produces the single-frequency behavior in between level crossings seen in Fig. 8(a). In fact, when S mixing is artificially suppressed, the autocorrelation of n_z is not characterized by a single-frequency any more [see Fig. 8 (lower panel)].

V. CONCLUSIONS

The spin dynamics of the Fe_{10} wheel was investigated by inelastic neutron scattering, and analyzed using a microscopic model. Difficulties related with the dimension of the Hilbert space were overcome by exploiting both the irreducible tensor operator technique and the Lanczos algorithm. Intracluster dipolar interactions are found to be the main source of axial anisotropy, providing about 70% of the total anisotropy. Fe_{10} was proposed as one of the best candidate systems to observe tunneling of the Néel vector. Our results allow us to directly probe the zero-field autocorrelation of the Néel vector, and show that a tunneling scenario for this quantity is only approximately valid. In addition, the remarkable role of S mixing in the Néel vector dynamics was demonstrated.

ACKNOWLEDGMENTS

This work was partly supported by Ministero dell'Università e della Ricerca Scientifica e Tecnologica, FIRB Project RBNE01YLKN and by EPSRC(UK). This work utilized facilities supported in part by the National Science Foundation under Agreement No. DMR-0086210.

[1] A. Chiolero and D. Loss, Phys. Rev. Lett. **80**, 169 (1998).
[2] M. N. Leuenberger and D. Loss, Nature (London) **410**, 789 (2001).
[3] F. Meier and D. Loss, Phys. Rev. B **64**, 224411 (2001).
[4] B. Normand, X. Wang, X. Zotos, and D. Loss, Phys. Rev. B **63**, 184409 (2001).
[5] I. Rudra, S. Ramasesha, and D. Sen, Phys. Rev. B **66**, 014441 (2002).
[6] A. Honecker, F. Meier, D. Loss, and B. Normand, Eur. Phys. J. B **27**, 487 (2002).
[7] M. N. Leuenberger, F. Meier, and D. Loss, Chem. Monthly **134**, 217 (2003).
[8] S. Carretta, J. van Slageren, T. Guidi, E. Liviotti, C. Mondelli, D. Rovai, A. Cornia, A. L. Dearden, M. Affronte, C. D. Frost, R. E. P. Winpenny, D. Gatteschi, G. Amoretti, and R. Caciuffo, Phys. Rev. B **67**, 094405 (2003).
[9] O. Waldmann, T. Guidi, S. Carretta, C. Mondelli, and A. L. Dearden, Phys. Rev. Lett. **91**, 237202 (2003).
[10] O. Waldmann, C. Dobe, H. Mutka, A. Furrer, and H. U. Güdel, cond-mat/0410447.
[11] O. Waldmann, J. Schülein, R. Koch, P. Müller, I. Bernt, R. W. Saalfrank, H. P. Andres, H. U. Güdel, and P. Allenspach, Inorg. Chem. **38**, 5879 (1999).
[12] K. L. Taft, C. D. Delfs, G. C. Papefthymiou, S. Foner, D. Gatteschi, and S. J. Lippard, J. Am. Chem. Soc. **116**, 823 (1994).
[13] A. Caneschi, A. Cornia, A. C. Fabretti, S. Foner, D. Gatteschi, R. Grandi, and L. Schenetti, Chem.-Eur. J. **2**, 1379 (1996).
[14] A. Cornia, A. G. M. Jansen, and M. Affronte, Phys. Rev. B **60**, 12 177 (1999).
[15] J. Bruno and R. J. Silbey, J. Phys. Chem. A **104**, 596 (2000).
[16] M.-H. Julien, Z. H. Jang, A. Lascialfari, F. Borsa, M. Horvatić, A. Caneschi, and D. Gatteschi, Phys. Rev. Lett. **83**, 227 (1999).
[17] A. Cornia, A. Fort, M. G. Pini, and A. Rettori, Europhys. Lett. **50**, 88 (2000).
[18] M. Affronte, J. C. Lasjaunias, A. Cornia, and A. Caneschi, Phys. Rev. B **60**, 1161 (1999).
[19] J. R. D. Copley and J. C. Cook, Chem. Phys. **292**, 477 (2003).
[20] Go to http://www.ncnr.nist.gov/dave.
[21] E. Liviotti, S. Carretta, and G. Amoretti, J. Chem. Phys. **117**, 3361 (2002).
[22] J. Schnack and M. Luban, Phys. Rev. B **63**, 014418 (2001).
[23] O. Waldmann, Phys. Rev. B **65**, 024424 (2002).
[24] O. Waldmann, Phys. Rev. B **61**, 6138 (2000).
[25] O. Waldmann, Phys. Rev. B **68**, 174406 (2002).
[26] R. Caciuffo, T. Guidi, G. Amoretti, S. Carretta, E. Liviotti, P. Santini, C. Mondelli, G. Timco, C. A. Muryn, and R. E. P. Winpenny, Phys. Rev. B (to be published).
[27] The semiclassical results based on Eq. (2) are obtained by assuming single-site uniaxial anisotropy only, while the real anisotropy is biaxial and originates also from dipolar interactions. All our quantum calculations are based on the true microscopic Hamiltonian. As far as the tunneling of **n** is concerned, this Hamiltonian produces essentially the same physics as the simplified model with single-site axial anisotropy only, but with a value of d 3.45 times larger. This yields $\mathcal{S}_0 \sim 4.2$.